Experimental observation of magnetic poles inside bulk magnets via $\mathbf{q} \neq 0$ Fourier modes of magnetostatic field

2014 New J. Phys. 16 123031

(http://iopscience.iop.org/1367-2630/16/12/123031)

New Journal of Physics
The open access journal at the forefront of physics
Deutsche Physikalische Gesellschaft DPG | IOP Institute of Physics

Experimental observation of magnetic poles inside bulk magnets via q ≠ 0 Fourier modes of magnetostatic field

Élio A Périgo[1], Elliot P Gilbert[2], Konstantin L Metlov[3] and Andreas Michels[1]

[1] Physics and Materials Science Research Unit, University of Luxembourg, 162A Avenue de la Faïencerie, L-1511 Luxembourg, Luxembourg
[2] Bragg Institute, ANSTO, Locked Bag 2001, Kirrawee DC, NSW 2232, Australia
[3] Donetsk Institute for Physics and Technology NAS, Donetsk 83114, Ukraine
E-mail: andreas.michels@uni.lu

Received 23 July 2014, revised 9 October 2014
Accepted for publication 18 November 2014
Published 15 December 2014

New Journal of Physics **16** (2014) 123031

doi:10.1088/1367-2630/16/12/123031

Abstract

The pole-avoidance principle of magnetostatics results in an angular anisotropy of the magnetic neutron scattering cross section $d\Sigma_M/d\Omega$. For the case of a sintered Nd–Fe–B permanent magnet, we report the experimental observation of a 'spike' in $d\Sigma_M/d\Omega$ along the forward direction. The spike implies the presence of long-wavelength magnetization fluctuations on a length scale of at least 60 nm. Using micromagnetic theory, it is shown that this type of angular anisotropy is the result of the presence of unavoidable magnetic poles in the bulk of the magnet and is related to the $\mathbf{q} \neq 0$ Fourier modes of the magnetostatic field. Thus, our observation proves the existence of such modes.

Keywords: magnetic neutron scattering, magnetodipolar interaction, spin-ice compounds

1. Introduction

The dipole–dipole interaction is one of the most fundamental interactions in condensed-matter physics. For instance, the scattering of thermal neutrons by magnetic materials, the Overhauser effect in nuclear magnetic resonance and the related phenomenon of dynamic nuclear

polarization [1], or the appearance of van-der-Waals forces can all be described using the concept of the interaction between (electrical and magnetic) dipoles.

In recent years, the magnetodipolar interaction moved into the focus of attention within the framework of the study of so-called spin-ice compounds (Dy and Ho-based pyrochlores) (e.g. [2–11]). In these systems, it is possible to achieve a substantial magnetic-pole separation such that individual poles behave like magnetic monopoles, in this way realizing Dirac's hypothesis in practice. Magnetic monopoles in spin-ice compounds give rise to frustration, dipolar ferromagnetic coupling, exotic field-induced phase transitions and unusual glassiness (see, e.g. [12] for a recent review).

Besides their long-range nature, dipole–dipole interactions are anisotropic in the sense that the energy of a given arrangement of dipoles depends not only on the distance between them but also on their orientation. A textbook example is the energy of two parallel-aligned magnetic moments $\mathbf{m}_1$ and $\mathbf{m}_2$, which takes on values of $\frac{\mu_0}{4\pi}\frac{m_1 m_2}{r^3}$ for the $\uparrow\uparrow$ state and $-\frac{\mu_0}{2\pi}\frac{m_1 m_2}{r^3}$ for the $\rightarrow\rightarrow$ arrangement, where $r = |\mathbf{r}|$ denotes the distance between $\mathbf{m}_1$ and $\mathbf{m}_2$ and $\mu_0 = 4\pi 10^{-7}\,\mathrm{Tm\,A^{-1}}$.

Unlike spin-ice compounds, for macroscopic bulk magnets with $\sim 10^{23}$ atomic spins per cm^3, the picture of discrete magnetic moments becomes a burden. It is more convenient to describe their magnetization state by a continuous magnetization vector field $\mathbf{M}(\mathbf{r})$, and to associate the interaction of the discrete atomic magnetic moments—within the Lorentz continuum approximation—with the magnetostatic self-interaction energy $E_m \geqslant 0$ [13–15]

$$E_m = +\frac{\mu_0}{2}\int \mathbf{H}_d^2\,\mathrm{d}V, \tag{1}$$

where $\mathbf{H}_d(\mathbf{r})$ denotes the magnetostatic field and the integral is taken over all space. Since the sources of $\mathbf{H}_d$ are inhomogeneities of $\mathbf{M}$ (either in orientation and/or in magnitude), positiveness of E_m (or, strictly speaking, the existence of its lower bound, achieved only in the absence of sources) implies that the magnetodipolar interaction tries to avoid any sort of magnetic volume ($-\nabla\cdot\mathbf{M}$) or surface ($\mathbf{n}\cdot\mathbf{M}$) poles; this is the content of the so-called pole-avoidance principle.

Similarly to the poles themselves, the field $\mathbf{H}_d(\mathbf{r})$ can be decomposed into the surface demagnetizing field $\mathbf{H}_d^s(\mathbf{r})$ and into the magnetostatic field $\mathbf{H}_d^b(\mathbf{r})$ related to volume charges, i.e. $\mathbf{H}_d(\mathbf{r}) = \mathbf{H}_d^s(\mathbf{r}) + \mathbf{H}_d^b(\mathbf{r})$ [14]. For uniformly magnetized bodies of ellipsoidal shape, $\mathbf{H}_d^s$ is *uniform* inside the material; if furthermore $\mathbf{M}$ is aligned along a principal axis of the sample (assumed in the following to be the z-direction of a Cartesian coordinate system), then $\mathbf{H}_d^s = -NM_s\mathbf{e}_z$, where N denotes the corresponding demagnetizing factor and $M_s = |\mathbf{M}|$ is the saturation magnetization. In the presence of a uniform applied magnetic field $\mathbf{H}_0 = H_0\mathbf{e}_z$, both fields $\mathbf{H}_d^s$ and $\mathbf{H}_0$ can be superposed to yield the (uniform) internal magnetic field $H_i = |\mathbf{H}_i| = H_0 - NM_s$. Under these assumptions and with reference to the title of the paper, the field $\mathbf{H}_d^s$ may then be considered as the macroscopic $\mathbf{q} = 0$ Fourier component of $\mathbf{H}_d$.

The $\mathbf{q} \neq 0$ Fourier component of $\mathbf{H}_d(\mathbf{r})$, denoted as $\mathbf{h}_d^b(\mathbf{q})$, is obtained by solving Maxwell's magnetostatic equations (no currents) $\nabla\cdot\mathbf{B} = 0$, $\nabla\times\mathbf{H}_d = 0$, and $\mathbf{B} = \mu_0(\mathbf{H}_d + \mathbf{M})$ as [16]

$$\mathbf{h}_d^b(\mathbf{q}) = -\frac{\mathbf{q}\left[\mathbf{q}\cdot\widetilde{\mathbf{M}}(\mathbf{q})\right]}{q^2}, \tag{2}$$

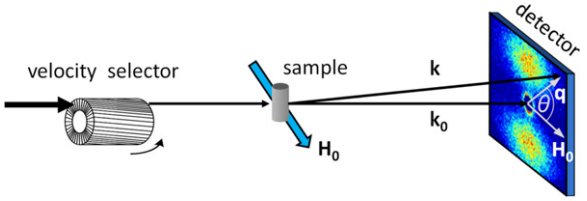

Figure 1. Sketch of the neutron-scattering setup.

where $\widetilde{\mathbf{M}}(\mathbf{q})$ represents the Fourier transform of $\mathbf{M}(\mathbf{r})$. Equation (2) implies that pole avoidance prefers magnetic structures with Fourier modes $\widetilde{\mathbf{M}}$ *normal* to the wave (or scattering) vector $\mathbf{q}$. Moreover, the anisotropic character of the dipole–dipole interaction, which is embodied in equation (2), can also be expected to induce anisotropic features in the magnetic neutron scattering cross section, which is a function of $\widetilde{\mathbf{M}}(\mathbf{q})$.

Here, we report the results of neutron-scattering experiments on a Nd–Fe–B magnet which reveal a 'spike' in the magnetic neutron scattering cross section. We will demonstrate that the origin of the spike is related to the Fourier coefficient $\mathbf{h}_d^b(\mathbf{q})$ of the magnetostatic field and that it is a direct manifestation of pole avoidance (flux closure) in the bulk of magnetic materials.

2. Experiment

The neutron-scattering experiments were carried out at 295 K at the instrument Quokka [17] at the Australian Nuclear Science and Technology Organisation. Figure 1 depicts a sketch of the experimental setup. Incident unpolarized neutrons with a mean wavelength of $\lambda = 4.8$ Å ($\Delta\lambda/\lambda = 10$ % (FWHM)) were selected by means of a velocity selector. The magnetic field $\mathbf{H}_0$ at the sample position was applied perpendicular to the incoming neutron beam (wave vector $\mathbf{k}_0$). Scattered neutrons were counted on a two-dimensional position-sensitive detector. Neutron data were corrected for background (empty sample holder) scattering, transmission, and detector efficiency and set to absolute units using a calibrated attenuated direct-beam measurement. The sample under study was a sintered isotropic (i.e. untextured) Nd–Fe–B permanent magnet (grade: N42); the neutron sample was prepared in the form of a circular disc with a diameter of 22.0 mm and a thickness of 512 μm ($N \cong 0.0178$).

3. Results and discussion

Figure 2 displays the experimental unpolarized (nuclear and magnetic) macroscopic differential scattering cross section $\mathrm{d}\Sigma/\mathrm{d}\Omega$ of a Nd–Fe–B magnet at several applied-field values; figure 3 shows $\mathrm{d}\Sigma/\mathrm{d}\Omega$ at a fixed momentum transfer of $q = 0.10 \pm 0.02\ \mathrm{nm}^{-1}$ as a function of the azimuthal angle $\theta = \measuredangle(\mathbf{q}, \mathbf{H}_0)$. On reducing the field starting from 10 T, where a $\sin^2\theta$-type anisotropy with maxima perpendicular to $\mathbf{H}_0$ is visible (figure 2(a)), one clearly observes the emergence of a spike in $\mathrm{d}\Sigma/\mathrm{d}\Omega$ along the field direction ($\theta = 0°$ and $\theta = 180°$) at fields below about 4 T and extending even to negative values (figures 2(b)–(d)). In the following, we provide a more detailed discussion of the origin of this angular spike anisotropy in $\mathrm{d}\Sigma/\mathrm{d}\Omega$ in terms of the continuum theory of micromagnetics.

The static equations of micromagnetics for the bulk of magnetic media can be conveniently expressed as a balance-of-torques equation [13–15],

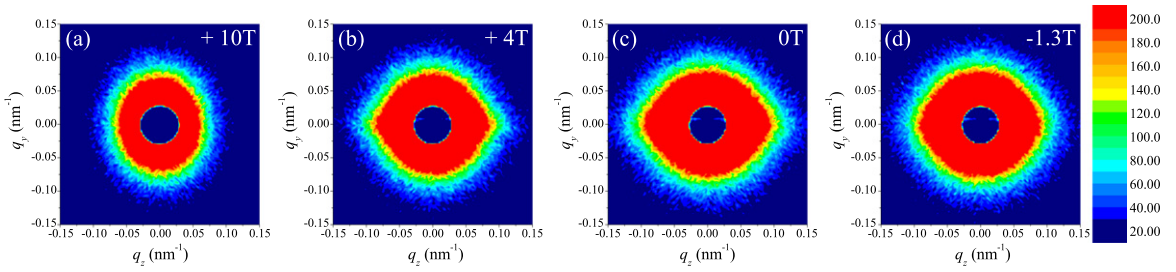

Figure 2. Color-coded map of the experimental unpolarized scattering intensity $d\Sigma/d\Omega$ of a sintered (untextured) Nd–Fe–B permanent magnet at selected applied magnetic fields (see insets) ($\mathbf{k}_0 \perp \mathbf{H}_0$). $\mathbf{H}_0$ is horizontal; for the definition of the angle θ, see figure 1. The central blue spots mask the region of the beam stop.

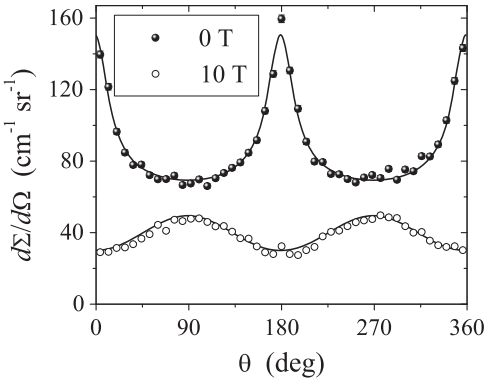

Figure 3. $d\Sigma/d\Omega$ of a sintered Nd–Fe–B magnet as a function of the azimuthal angle θ at fixed $q = 0.10 \pm 0.02\,\mathrm{nm}^{-1}$ and at two selected applied magnetic fields (see inset). Solid lines are theoretical predictions (see text).

$$\mathbf{M} \times \left(\mathbf{H}_0 + \mathbf{H}_d + \mathbf{H}_p + \frac{2A}{\mu_0 M_s^2} \nabla^2 \mathbf{M} \right) = 0, \tag{3}$$

where $\mathbf{H}_p(\mathbf{r})$ and $\frac{2A}{\mu_0 M_s^2} \nabla^2 \mathbf{M}(\mathbf{r})$ denote, respectively, the magnetic anisotropy field and the exchange field (A is the exchange-stiffness constant). Equation (3) expresses the fact that at static equilibrium the torque on $\mathbf{M}$ due to the effective field term (in the brackets) vanishes everywhere inside the material.

At large applied fields $\mathbf{H}_0 \| \mathbf{e}_z$, one can linearize equation (3) and find closed-form expressions for the two independent transversal magnetization components M_x and M_y. In Fourier space, and with respect to neutron scattering at small angles, where one can neglect the component of the scattering vector along the incident beam and $\mathbf{q} \cong (0, q_y, q_z) = q\,(0, \sin\theta, \cos\theta)$ (compare figure 1), the solutions for $\widetilde{M}_x$ and $\widetilde{M}_y$ are [18]:

$$\widetilde{M}_x(\mathbf{q}) = M_s \frac{h_x(\mathbf{q})}{H_{\mathrm{eff}}}, \tag{4}$$

$$\widetilde{M}_y(\mathbf{q}) = M_s \frac{h_y(\mathbf{q}) - \widetilde{M}_z(\mathbf{q}) \sin\theta \cos\theta}{H_{\text{eff}} + M_s \sin^2\theta}, \tag{5}$$

where $\mathbf{h}(\mathbf{q}) = (h_x(\mathbf{q}), h_y(\mathbf{q}), 0)$ denotes the Fourier coefficient of the magnetic anisotropy field $\mathbf{H}_p(\mathbf{r})$, which varies as a function of the position inside the material and produces nanoscale spin disorder. The Fourier coefficient of the longitudinal magnetization, $\widetilde{M}_z(\mathbf{q})$, is proportional to the jump ΔM in the magnitude of the magnetization at internal particle–matrix interfaces. The quantity $H_{\text{eff}}(q, H_i) = H_i\left(1 + l_H^2 q^2\right)$ depends on the internal (applied) field H_i, on $q = |\mathbf{q}|$, and on the exchange length of the field $l_H(H_i) = \sqrt{2A/(\mu_0 M_s H_i)}$.

The important point to realize is that the terms $\widetilde{M}_z(\mathbf{q}) \sin\theta \cos\theta$ and $M_s \sin^2\theta$ in equation (5) are due to the magnetodipolar interaction. To be more precise, these terms are due to the inclusion of the $\mathbf{q} \neq 0$ Fourier component of the magnetostatic field, $\mathbf{h}_d^b(\mathbf{q})$ (equation (2)). As we will see below, these contributions decisively determine the angular anisotropy of the elastic (small-angle) neutron scattering (SANS) cross section $\mathrm{d}\Sigma/\mathrm{d}\Omega$, which, for unpolarized neutrons and the above scattering geometry ($\mathbf{k}_0 \perp \mathbf{H}_0$), reads [19, 20]

$$\begin{aligned}\frac{\mathrm{d}\Sigma}{\mathrm{d}\Omega}(\mathbf{q}) = \frac{8\pi^3}{V}\Big(&\left|\widetilde{N}\right|^2 + b_H^2\left|\widetilde{M}_x\right|^2 + b_H^2\left|\widetilde{M}_y\right|^2 \cos^2\theta \\ &+ b_H^2\left|\widetilde{M}_z\right|^2 \sin^2\theta - b_H^2\left(\widetilde{M}_y\widetilde{M}_z^* + \widetilde{M}_y^*\widetilde{M}_z\right)\sin\theta\cos\theta\Big);\end{aligned} \tag{6}$$

V is the scattering volume, $b_H = 2.9 \times 10^8\,\mathrm{A^{-1}m^{-1}}$, and $\widetilde{N}(\mathbf{q})$ is the Fourier coefficient of the nuclear scattering-length density; the asterisks '*' mark the complex-conjugated quantity. When equations (4) and (5) are inserted into equation (6), $\mathrm{d}\Sigma/\mathrm{d}\Omega$ can be expressed as [18]

$$\frac{\mathrm{d}\Sigma}{\mathrm{d}\Omega}(\mathbf{q}) = \frac{\mathrm{d}\Sigma_{\text{res}}}{\mathrm{d}\Omega}(\mathbf{q}) + \frac{\mathrm{d}\Sigma_M}{\mathrm{d}\Omega}(\mathbf{q}), \tag{7}$$

where

$$\frac{\mathrm{d}\Sigma_{\text{res}}}{\mathrm{d}\Omega}(\mathbf{q}) = \frac{8\pi^3}{V}\left(\left|\widetilde{N}\right|^2 + b_H^2\left|\widetilde{M}_z\right|^2 \sin^2\theta\right) \tag{8}$$

represents the (nuclear and magnetic) residual SANS cross section, which is measured at complete magnetic saturation (infinite field), and

$$\frac{\mathrm{d}\Sigma_M}{\mathrm{d}\Omega}(\mathbf{q}) = S_H(\mathbf{q})\, R_H\left(q, \theta, H_i\right) + S_M(\mathbf{q})\, R_M\left(q, \theta, H_i\right) \tag{9}$$

is the spin-misalignment SANS cross section, which decomposes into a contribution $S_H R_H$ due to perturbing magnetic anisotropy fields and a part $S_M R_M$ related to magnetostatic fields. The anisotropy-field scattering function $S_H(\mathbf{q}) = \frac{8\pi^3}{V} b_H^2 |h|^2$ depends on the Fourier coefficient $h(\mathbf{q})$ of the magnetic anisotropy field, whereas the scattering function of the longitudinal magnetization $S_M(\mathbf{q}) = \frac{8\pi^3}{V} b_H^2 |\widetilde{M}_z|^2$ provides information on the magnitude $\Delta M \propto \widetilde{M}_z$ of the magnetization jump at internal interfaces. The corresponding (dimensionless) micromagnetic response functions are

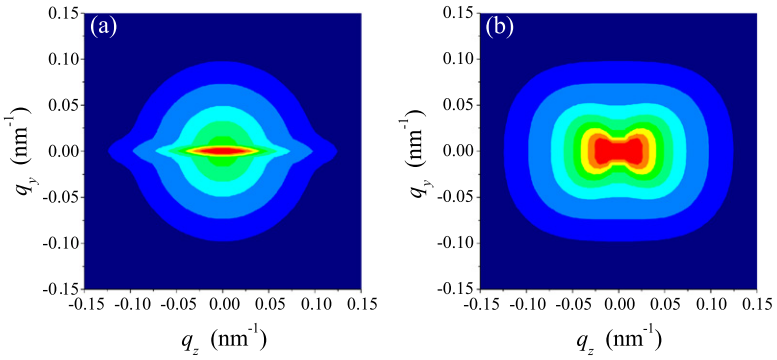

Figure 4. Impact of the magnetodipolar term $M_s \sin^2\theta$ on the spin-misalignment neutron scattering cross section $\mathrm{d}\Sigma_M/\mathrm{d}\Omega$ (equation (9) with $S_H(q) = S_M(q)$) ($\mathbf{k}_0 \perp \mathbf{H}_0$). (a) $\mathrm{d}\Sigma_M/\mathrm{d}\Omega$ with $M_s \sin^2\theta$; (b) $\mathrm{d}\Sigma_M/\mathrm{d}\Omega$ without $M_s \sin^2\theta$ ($\mu_0 H_i = 0.01$ mT). Materials parameters: $\mu_0 M_s = 1.44$ T; $A = 5.9$ pJ m^{-1}. Red–yellow color corresponds to 'high intensity' and blue color to 'low intensity'.

$$R_H(q, \theta, H_i) = \frac{p^2}{2}\left(1 + \frac{\cos^2\theta}{\left(1 + p\sin^2\theta\right)^2}\right) \tag{10}$$

and

$$R_M(q, \theta, H_i) = \frac{p^2 \sin^2\theta \cos^4\theta}{\left(1 + p\sin^2\theta\right)^2} + \frac{2p\sin^2\theta\cos^2\theta}{1 + p\sin^2\theta}, \tag{11}$$

where $p(q, H_i) = M_s/H_{\mathrm{eff}}(q, H_i)$. For polycrystalline bulk ferromagnets, the functions $|\widetilde{N}|^2$, $|\widetilde{M}_z|^2$, $|h|^2$ and, hence, $|\widetilde{M}_x|^2$ (compare equation (4)) are all isotropic, i.e. they depend only on the magnitude q of the scattering vector, not on the angle θ [21, 22]. Therefore, any angular (θ) anisotropy that becomes visible in $\mathrm{d}\Sigma/\mathrm{d}\Omega$ (equation (6)) is a consequence of the trigonometric functions in conjunction with scattering terms $\propto \widetilde{M}_y^2$ and $-2\widetilde{M}_y\widetilde{M}_z$, which by virtue of equations (2) and (5) depend explicitly on the angle θ. Then, depending on the values of q, H_i, and on the ratio of S_H to S_M, a variety of different SANS patterns can be observed on a two-dimensional detector (compare figures 2 and 3 in [18]).

Note, however, that for the hard magnetic material under study, the term $S_M R_M$ in $\mathrm{d}\Sigma_M/\mathrm{d}\Omega$ is less important than the anisotropy-field related contribution $S_H R_H$. In fact, in the experimental neutron data (figure 2), we do not observe maxima along the diagonals of the detector, as one would expect if the term $S_M R_M$ significantly contributes to the magnetic scattering (compare equation (11)).

In order to demonstrate in particular the effect of the magnetodipolar term $M_s \sin^2\theta$ in the denominator of equation (5) ($p\sin^2\theta$ in equations (10) and (11)) on the spin-misalignment neutron scattering cross section $\mathrm{d}\Sigma_M/\mathrm{d}\Omega$, we show in figure 4 $\mathrm{d}\Sigma_M/\mathrm{d}\Omega$ with (figure 4(a)) and without (figure 4(b)) this term [18]. It is clearly seen that the inclusion of the magnetostatic term $M_s \sin^2\theta$ in $\mathrm{d}\Sigma_M/\mathrm{d}\Omega$ gives rise to a sharp spike in the direction parallel (and anti-parallel) to the applied-field direction; the term vanishes for $\theta = 0°$ and in this way increases the contribution (amplitude) of the $\widetilde{M}_y$ Fourier coefficient to $\mathrm{d}\Sigma_M/\mathrm{d}\Omega$. The spike (or flying-saucer-type pattern)

was first predicted by Weissmüller *et al* [23]. Note also that the $d\Sigma_M/d\Omega$ data that are shown in figure 4 are only qualitative with respect to absolute values and $|\mathbf{q}|$-dependence; adding (realistic) isotropic nuclear SANS ($\sim|\widetilde{N}|^2$) and longitudinal magnetic scattering ($\sim|\widetilde{M}_z|^2 \sin^2\theta$) to $d\Sigma_M/d\Omega$ in order to arrive at the total (nuclear and magnetic) $d\Sigma/d\Omega$ (as in the experiment) does not change the result shown in figure 4. Since the spike anisotropy is observed for a wide range of applied magnetic fields, starting already at around ±6 T (data not shown), where the sample is essentially in the approach-to-saturation regime, we believe that other magnetization textures (e.g. Bloch or Néel-type structures) play only a minor role for the anisotropy of the magnetic SANS cross section.

Furthermore, we note that when equations (7)–(11) are evaluated at a fixed q and H_i and the angle θ is treated as the independent variable, then the cross section is of the form $d\Sigma/d\Omega = a_1 + a_2 \sin^2\theta + a_3 R_H(\theta) + a_4 R_M(\theta)$, where the a_i are adjustable parameters (solid lines in figure 3); treating the exchange-stiffness constant A (in the expression for H_{eff} and, hence, in $p(q, H_i)$) as an additional adjustable parameter, results in $A = 5.9 \pm 0.1$ pJ m^{-1}, which compares favorably with literature data [24].

4. Summary and conclusions

The excellent qualitative agreement between our experimental data (figures 2 and 3) and the micromagnetic simulation (figure 4) strongly suggests that the observed spike anisotropy in $d\Sigma/d\Omega$ of a Nd–Fe–B magnet is a consequence of unavoidable magnetic poles, existing in the bulk. In other words, the spike is due to the presence of $\mathbf{q} \neq 0$ Fourier modes of the magnetostatic field, here, on a mesoscopic length scale of $\sim 2\pi/0.1\ \text{nm}^{-1} \cong 60$ nm and larger. The results underline the importance of the magnetodipolar interaction for understanding magnetic SANS. Since the spike pattern bears similarities with the dipolar correlations in the pyrochlores, where characteristic cone-shaped intensity patterns (pinch points) were observed by means of diffuse neutron diffraction [7, 8], it would be of interest to search for the signature of the spike on a more microscopic length scale, as it becomes visible in the vicinity of Bragg peaks.

Acknowledgments

Financial support by the National Research Fund of Luxembourg (project no. FNR/A09/01) and by the University of Luxembourg (INTERFACE 2012) is gratefully acknowledged. We also thank Paolo Imperia, Norman Booth, and Gene Davidson for sample-environment support, and Ferdi Franceschini and Norman Xiong for optimization of remote communication and control of the cryomagnet.

References

[1] Abragam A 2002 *Principles of Nuclear Magnetism* (Oxford: Oxford University Press)
[2] Siddharthan R, Shastry B S, Ramirez A P, Hayashi A, Cava R J and Rosenkranz S 1999 *Phys. Rev. Lett.* **83** 1854–7
[3] Bramwell S T *et al* 2001 *Phys. Rev. Lett.* **87** 047205
[4] Wiebe C R, Gardner J S, Kim S J, Luke G M, Wills A S, Gaulin B D, Greedan J E, Swainson I, Qiu Y and Jones C Y 2004 *Phys. Rev. Lett.* **93** 076403

[5] Mirebeau I, Apetrei A, Rodríguez-Carvajal J, Bonville P, Forget A, Colson D, Glazkov V, Sanchez J P, Isnard O and Suard E 2005 *Phys. Rev. Lett.* **94** 246402
[6] Castelnovo C, Moessner R and Sondhi S L 2008 *Nature* **451** 42
[7] Morris D J P *et al* 2009 *Science* **326** 411–4
[8] Fennell T, Deen P P, Wildes A R, Schmalzl K, Prabhakaran D, Boothroyd A T, Aldus R J, McMorrow D F and Bramwell S T 2009 *Science* **326** 415–7
[9] Bramwell S T, Giblin S R, Calder S, Aldus R, Prabhakaran D and Fennell T 2009 *Nature* **461** 956
[10] Borzi R A, Slobinsky D and Grigera S A 2013 *Phys. Rev. Lett.* **111** 147204
[11] Nisoli C, Moessner R and Schiffer P 2013 *Rev. Mod. Phys.* **85** 1473–90
[12] Castelnovo C, Moessner R and Sondhi S L 2012 *Annu. Rev. Condens. Matter Phys.* **3** 35
[13] Brown W F Jr 1963 *Micromagnetics* (New York: Interscience)
[14] Aharoni A 1996 *Introduction to the Theory of Ferromagnetism* 2nd edn (Oxford: Clarendon)
[15] Kronmüller H and Fähnle M 2003 *Micromagnetism and the Microstructure of Ferromagnetic Solids* (Cambridge: Cambridge University Press)
[16] Herring C and Kittel C 1951 *Phys. Rev.* **81** 869
[17] Gilbert E P, Schulz J C and Noakes T J 2006 *Physica* B **385–386** 1180
[18] Honecker D and Michels A 2013 *Phys. Rev.* B **87** 224426
[19] Michels A and Weissmüller J 2008 *Rep. Prog. Phys.* **71** 066501
[20] Michels A 2014 *J. Phys.: Condens. Matter* **26** 383201
[21] Honecker D, Ferdinand A, Döbrich F, Dewhurst C D, Wiedenmann A, Gómez-Polo C, Suzuki K and Michels A 2010 *Eur. Phys. J.* B **76** 209–13
[22] Erokhin S, Berkov D, Gorn N and Michels A 2012 *Phys. Rev.* B **85** 134418
[23] Weissmüller J, McMichael R D, Michels A and Shull R D 1999 *J. Res. Natl Inst. Stand. Technol.* **104** 261
[24] Skomski R 2003 *J. Phys.: Condens. Matter* **15** R841